

# Theory for doping trends in titanium oxypnictide superconductors

Han-Xiang Xu,<sup>1</sup> Daniel Guterding,<sup>2</sup> and Harald O. Jeschke<sup>1</sup>

<sup>1</sup>Research Institute for Interdisciplinary Science, Okayama University, Okayama 700-8530, Japan

<sup>2</sup>Fachbereich Mathematik, Naturwissenschaften und Datenverarbeitung,

Technische Hochschule Mittelhessen, Wilhelm-Leuschner-Straße 13, 61169 Friedberg, Germany

(Dated: March 7, 2022)

A family of titanium oxypnictide materials  $\text{BaTi}_2\text{Pn}_2\text{O}$  ( $\text{Pn}$  = pnictogen) becomes superconducting when a charge and/or spin density wave is suppressed. With hole doping, isovalent doping and pressure, a whole range of tuning parameters is available. We investigate how charge doping controls the superconducting transition temperature  $T_c$ . To this end, we use experimental crystal structure data to determine the electronic structure and Fermi surface evolution along the doping path. We show that a naive approach to calculating  $T_c$  via the density of states at the Fermi level and the McMillan formula systematically fails to yield the observed  $T_c$  variation. On the other hand, spin fluctuation theory pairing calculations allow us to consistently explain the  $T_c$  increase with doping. All alkali doped materials  $\text{Ba}_{1-x}\text{A}_x\text{Ti}_2\text{Sb}_2\text{O}$  ( $\text{A}=\text{Na}, \text{K}, \text{Rb}$ ) are described by a sign-changing  $s$ -wave order parameter. Susceptibilities also reveal that the physics of the materials is controlled by a single Ti  $3d$  orbital.

*Introduction.*— The first layered titanium oxypnictides  $\text{Na}_2\text{Ti}_2\text{As}_2\text{O}$  and  $\text{Na}_2\text{Ti}_2\text{Sb}_2\text{O}$  were synthesized three decades ago [1] and discussed in terms of spin density wave (SDW) or charge density wave (CDW) behavior [2, 3]. Nine years ago, superconductivity was discovered in  $\text{BaTi}_2\text{Sb}_2\text{O}$  [4] and  $\text{BaTi}_2\text{Bi}_2\text{O}$  [5]. By analysis of the  $\text{BaTi}_2(\text{As}_{1-x}\text{Sb}_x)_2\text{O}$  solid solutions it quickly became apparent that superconductivity is favored by a suppression of the CDW/SDW phase [6, 7]. An extensive discussion of the phase transition observed in resistivity and magnetic susceptibility [2, 4, 8, 9] as well as thermoelectric power and Hall coefficient [10] concerns the question whether it should be characterized as a CDW transition or if it is in fact an SDW transition. Experimental evidence from nuclear magnetic resonance (NMR) [11] and muon spin relaxation ( $\mu\text{SR}$ ) [12, 13] does not completely resolve the question.

Shortly after the discovery of superconductivity, it was realized that both charge doping on the barium site and isovalent doping on the pnictogen site provide opportunities to control the superconductivity of  $\text{BaTi}_2\text{Sb}_2\text{O}$  in a significant range. Hole doping via alkali metals increases  $T_c$  from 1.2 K to 5.5 K in  $\text{Ba}_{1-x}\text{Na}_x\text{Ti}_2\text{Sb}_2\text{O}$  [9, 12], to 6.1 K in  $\text{Ba}_{1-x}\text{K}_x\text{Ti}_2\text{Sb}_2\text{O}$  [14], to 5.4 K in  $\text{Ba}_{1-x}\text{Rb}_x\text{Ti}_2\text{Sb}_2\text{O}$  [15] and to 4.4 K in  $\text{Ba}_{1-x}\text{Cs}_x\text{Ti}_2\text{Sb}_2\text{O}$  [16]. The maximum  $T_c$  is reached near an alkali content of  $x = 0.2$  to  $0.3$ . Isovalent doping via Sb/Bi mixing yields an intriguing two-dome  $T_c$  evolution with a non-superconducting or low  $T_c$  phase in between [6, 17]. More recently, pressure has been demonstrated to be an effective control parameter for superconductivity [18].

The nature of superconductivity in the titanium oxypnictides has been discussed since its discovery [19]. Experimentally, an  $s$ -wave gap has been inferred from nuclear quadrupole resonance (NQR) measurements [11], and specific heat is partially consistent with BCS expectations [20]. However,  $\mu\text{SR}$  measurements have been taken to indicate an unconventional pairing mech-

anism [21]. An NMR/NQR study points to significant differences in the superconductivity of  $\text{BaTi}_2\text{Sb}_2\text{O}$  and  $\text{BaTi}_2\text{Bi}_2\text{O}$  [22].

Theoretically, calculations of electron-phonon coupling have shown that the small transition temperature of  $\text{BaTi}_2\text{Sb}_2\text{O}$  can be explained by an electron-phonon mechanism [23]. On the other hand, based on the Fermi surfaces a sign-changing  $s$ -wave state has been predicted within spin fluctuation theory [24]. While the presence of magnetism has not been fully established in the titanium oxypnictides, an extensive density functional theory (DFT) study and symmetry analysis of the nematicity and charge order in  $\text{BaTi}_2\text{Sb}_2\text{O}$  have provided strong evidence that these materials cannot be understood without taking spin fluctuations into account [25].

While the electronic structure of individual titanium oxypnictide metals [26, 27] and superconductors [24, 28, 29] has been studied repeatedly, there is no theory for the evolution of properties with doping. Our study is intended to fill this gap. In this work, we show that we can consistently explain the evolution of the superconducting  $T_c$  with alkali doping using spin fluctuation theory and that the superconducting gap function has a sign-changing  $s$ -wave symmetry.

*Methods.*— We perform electronic structure calculations using the full potential local orbital (FPLO) basis set [30] and generalized gradient approximation (GGA) to the exchange and correlation potential [31]. We use smooth interpolations of lattice parameters of the  $P4/mmm$  space group (see Ref. 32, Fig. S1) and optimize the antimony positions within GGA. The charge doping is modeled via the virtual crystal approximation on the barium site. We use projective Wannier functions within FPLO [33] to obtain 26 band tight binding models including Ti  $3d$  and  $4s$ , Ba  $5d$ , Sb  $5p$  and O  $2p$  orbital characters. The models follow DFT bands and Fermi surfaces to a high degree of accuracy (see Ref. 32, Fig. S2). Based on the tight binding model, we calculate non-interacting susceptibilities  $\chi_{st}^{pq}(\mathbf{q})$ . We apply the random phase ap-

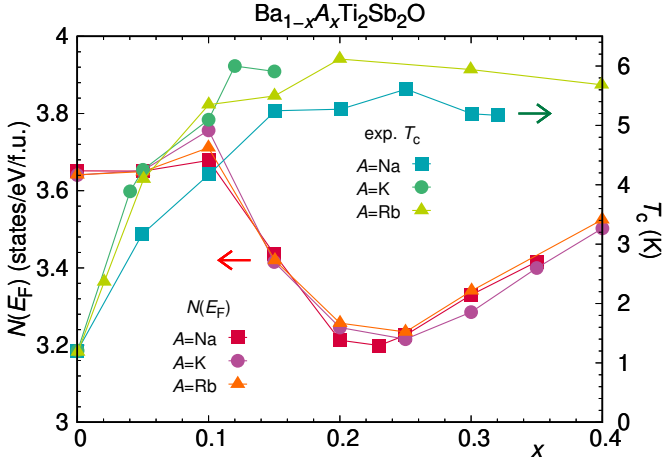


FIG. 1. (Color online) Density of states at the Fermi level  $N(E_F)$  shown together with experimental superconducting transition temperatures  $T_c$  for doping with three different alkali ions.  $T_c$  data are from Ref. 9 and 20 for Na doping, Ref. 14 for K doping, Ref. 15 for Rb doping.

proximation (RPA) and investigate the pairing instabilities within spin fluctuation theory by solving the gap equation on the Fermi surface [34–37]. Interaction parameters of  $U = 2$  eV (intra-orbital Coulomb repulsion),  $U' = 1$  eV (inter-orbital Coulomb repulsion),  $J = 0.5$  eV (Hund’s rule coupling and  $J' = 0.5$  eV (pair hopping), applied to Ti 3d orbitals, were used for RPA and pairing calculations.

**Results.-** The titanium oxypnictide superconductors have been treated as simple Bardeen, Cooper, Schrieffer (BCS) type superconductors in various experimental [4, 11, 15, 20, 38] and theoretical [23] studies. As a straight-forward attempt to understand the  $T_c$  tendencies, we extract the density of states at the Fermi level  $N(E_F)$  as a function of doping and try to apply the BCS formula  $T_c = 1.134 T_D \exp(-\frac{1}{VN(E_F)})$  (with Debye temperature  $T_D$  and electron-phonon coupling potential  $V$ ). Assuming constant  $T_D$  and  $V$ , this formula and its more sophisticated variants yield  $T_c$  trends that essentially follow  $N(E_F)$ .

Unfortunately, as Fig. 1 shows, there is very little similarity between  $N(E_F)$  and  $T_c$  evolution with doping. In the case of alkali doping of  $\text{BaTi}_2\text{Sb}_2\text{O}$ ,  $T_c$  quickly increases from  $T_c = 1.2$  K to a maximum that is reached between doping levels of  $x = 0.1$  to  $0.3$ . Meanwhile,  $N(E_F)$  remains constant until  $x = 0.1$  before going through a minimum at  $x = 0.23$  (Fig. 1). Based on this analysis, superconductivity in these materials could only be explained by an electron-phonon mechanism if the strength of electron-phonon coupling was extremely doping-dependent, so that it counteracts the unhelpful trends in  $N(E_F)$ . However, this seems very far-fetched. Therefore, we now turn to the possibility that the detailed evolution of the Fermi surface nesting provides doping dependencies strong enough to explain the evolution of  $T_c$  within spin fluctuation pairing theory.

Now we identify the most relevant orbitals at the Fermi level. In Fig. 2(a), we show the band structure and density of states of  $\text{BaTi}_2\text{Sb}_2\text{O}$  with Ti 3d and Sb 5p orbital character highlighted. The system is in general quite strongly hybridized and many orbitals contribute to the states close to the Fermi level. Taking a closer look, we find that the most relevant Ti 3d orbital for the low energy physics is  $3d_{xy}$  followed by  $3d_{xz,yz}$ . To visualize the Ti  $3d_{xy}$  orbital, we choose a local coordinate system for Ti where the  $z$ -axis points along the Ti-O bond and  $x$ - and  $y$ -axes point along Ti-Sb bonds. This is the natural local system to choose within the  $\text{TiO}_2\text{Sb}_4$  octahedron [27] (Fig. 2(b)), since it makes  $3d_{xz}$  and  $3d_{yz}$  degenerate. Fig. 2(c) shows the  $3d_{xy}$  Wannier functions at both titanium sites (Ti1 and Ti2) based on this coordinate choice.

We now analyze the Fermi surface evolution with alkali doping (Fig. 3). Only Ti  $3d_{xy}$  and Sb  $5p$  weights are highlighted (see Ref. 32, Fig. S3 for the other 3d weights). The  $\text{BaTi}_2\text{Sb}_2\text{O}$  Fermi surface is in excellent agreement with angle resolved photoemission (ARPES) experiments [39, 40] (see Ref. 32, Fig. S4). We see that the hole Fermi surfaces at  $X$  and  $Y$  grow with doping while the electron Fermi surface at  $M$  shrinks slightly. The Fermi surface at  $\Gamma$ , which is dominated by Sb  $5p$ , shows a rather complicated reconstruction as a function of doping.

In order to measure the relative importance of the Fermi surface changes, we turn to non-interacting susceptibilities calculated with the 26 band tight binding models on  $50 \times 50 \times 50$  integration meshes. Fig. 4 shows that the total susceptibility  $\chi_0$  is clearly peaked at  $\mathbf{q} = (\pi, 0, 0)$  (labeled  $X$ ) and  $\mathbf{q} = (0, \pi, 0)$  (labeled  $Y$ ). Previously, this has been noted based on the Lindhard function calculated without matrix elements [24, 28]. With alkali doping, the peaks at  $X$  and  $Y$  decrease, and they also move away from the high symmetry point towards  $\Gamma$ . At the same time,  $\chi_0$  at  $\mathbf{q} = (0, 0, 0)$  decreases. Interestingly, the doping trends of the total  $\chi_0$  and  $\chi_0^{xy}$  differ: While the ratio between  $X$  and  $\Gamma$  values of  $\chi_0$  hardly changes with doping, this ratio sharply increases for  $\chi_0^{xy}$  due to increases at  $X$  combined with decreases at  $\Gamma$ . This improved nesting is shown in Fig. 4(b) for Ti1, but equally applies to Ti2 where the  $Y$  to  $\Gamma$  ratio increases sharply. Furthermore, even though the Fermi surface shows substantial  $k_z$  dispersion, we can find the improved nesting also in the  $R$  to  $Z$  ratio. Meanwhile, the other orbitals, which are of some significance at the Fermi level ( $3d_{xz}$  and  $3d_{yz}$ ), have a comparatively featureless susceptibility (Fig. 4(c)) which uniformly decreases with doping. Note that calculations without matrix elements, i.e. solely based on the Lindhard function, do not contain the orbital-resolved information we just discussed. Since alkali doping seems to lead to an overall decrease in susceptibility, but strongly enhances the susceptibility of the Ti  $3d_{xy}$  orbitals, we can expect them to be the main actor in  $T_c$  changes with doping.

Since the similarity of susceptibilities along the  $k_z = 0$

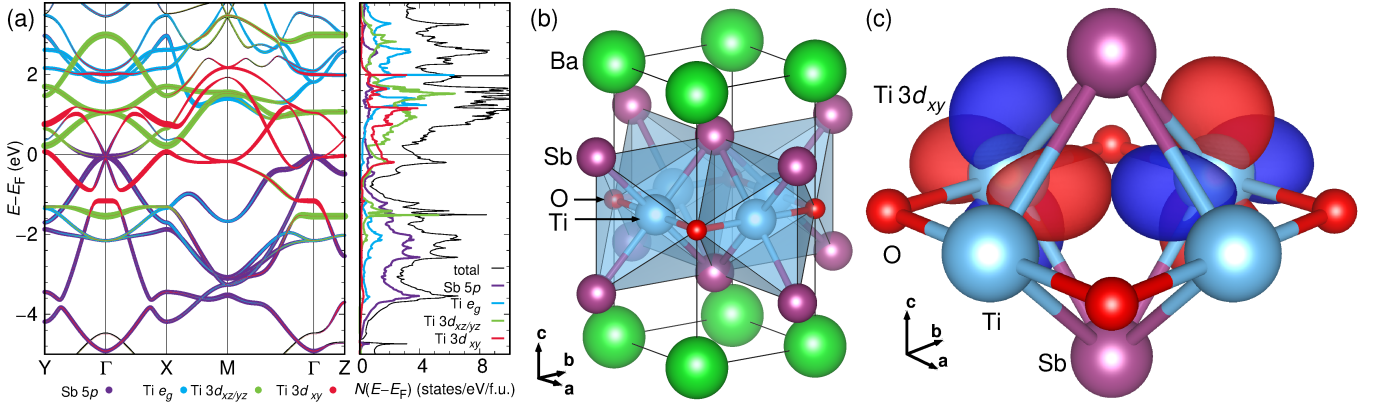


FIG. 2. (Color online) (a) GGA band structure and density of states of BaTi<sub>2</sub>Sb<sub>2</sub>O. (b) Crystal structure of BaTi<sub>2</sub>Sb<sub>2</sub>O with shaded TiO<sub>2</sub>Sb<sub>4</sub> octahedra. (c) Ti 3d<sub>xy</sub> Wannier functions within the Ti<sub>2</sub>Sb<sub>2</sub>O layer of BaTi<sub>2</sub>Sb<sub>2</sub>O.

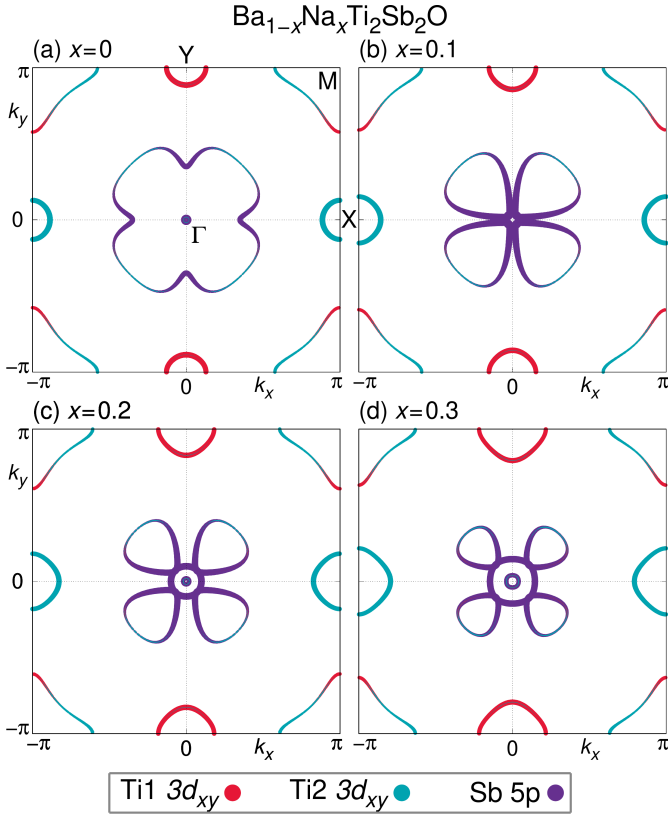


FIG. 3. (Color online) Fermi surfaces of Ba<sub>1-x</sub>Na<sub>x</sub>Ti<sub>2</sub>Sb<sub>2</sub>O at  $k_z = 0$  as function of doping level  $x$ , calculated within GGA.

and  $k_z = \pi$  paths in Fig. 4(a) indicates a high degree of two-dimensionality, we now focus on the 2D cuts of susceptibility and pairing in Fig. 5. It is clear that features of the non-interacting susceptibility  $\chi_0$  (see Ref. 32, Fig. S5), especially peaks at  $\mathbf{q} = (\pi, 0)$  and  $\mathbf{q} = (0, \pi)$ , are enhanced in the interacting susceptibility obtained by random phase approximation (Fig. 5(a)), reminiscent of single orbital system behaviour. These instabilities

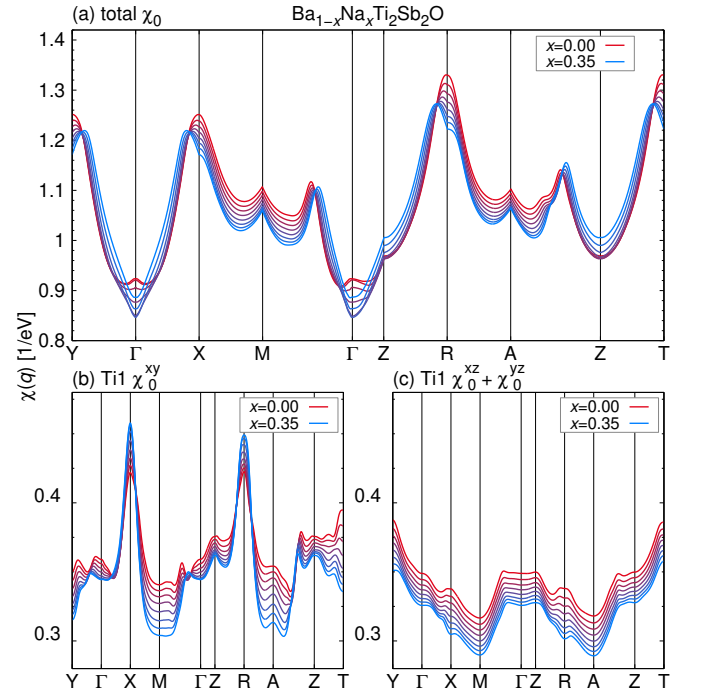


FIG. 4. (Color online) Non-interacting susceptibility of Ba<sub>1-x</sub>Na<sub>x</sub>Ti<sub>2</sub>Sb<sub>2</sub>O for eight doping levels  $x$ . (a) total, (b) 3d<sub>xy</sub> contribution from Ti1, (c) 3d<sub>xz</sub> and 3d<sub>yz</sub> contributions from Ti1.  $\mathbf{q} = (\pi, 0, 0)$  is labeled as X,  $\mathbf{q} = (0, \pi, 0)$  as Y,  $\mathbf{q} = (\pi, \pi, 0)$  as M,  $\mathbf{q} = (0, 0, \pi)$  as Z,  $\mathbf{q} = (0, \pi, \pi)$  as R,  $\mathbf{q} = (\pi, \pi, \pi)$  as A and  $\mathbf{q} = (\pi, 0, \pi)$  as T.

would now favor stripe-type magnetism which, however, has not been observed for BaTi<sub>2</sub>Sb<sub>2</sub>O [11–13].

Here, the  $(\pi, 0)$  and  $(0, \pi)$  instabilities favor a sign-changing  $s$ -wave superconducting order parameter: The gap functions corresponding to the leading eigenvalue  $\lambda$ , obtained using spin fluctuation theory, are shown in Fig. 5(c) and (d) for two different doping levels. Subleading  $d_{xy}$ - and  $d_{x^2-y^2}$ -type solutions have far smaller eigenvalues and are, therefore, irrelevant in

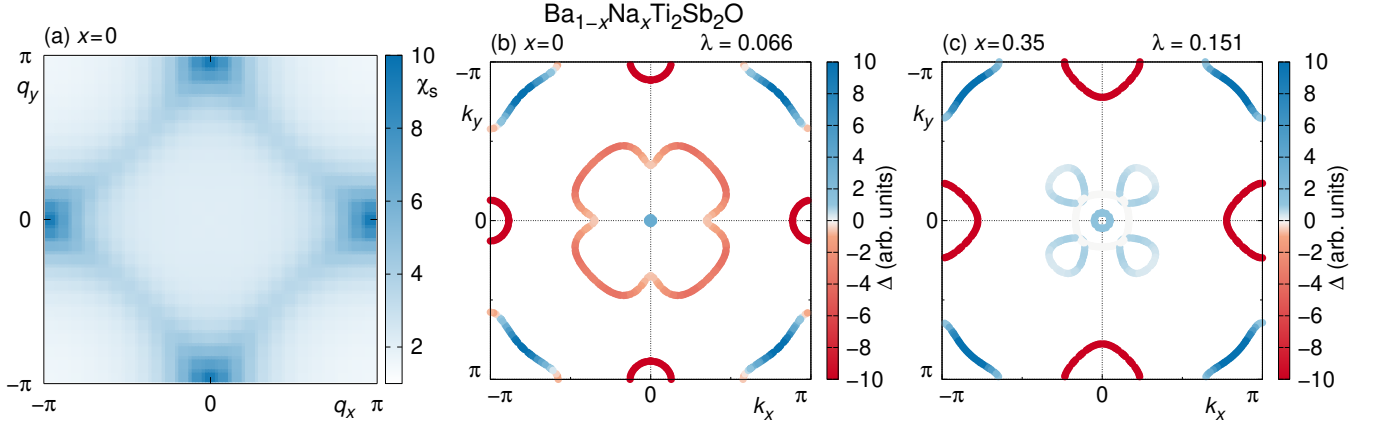


FIG. 5. (Color online) Two-dimensional susceptibility and gap functions of  $\text{Ba}_{1-x}\text{Na}_x\text{Ti}_2\text{Sb}_2\text{O}$ . (a) Spin susceptibility  $\chi_s$  calculated within RPA for  $x = 0$ , showing enhanced maxima at  $\mathbf{q} = (0, \pi)$  and  $\mathbf{q} = (\pi, 0)$ . (b) and (c) Eigen functions for the leading eigenvalue of the gap equation at zero doping (c) and at maximal doping (d). The sign-changing  $s$ -wave persists at all doping levels.

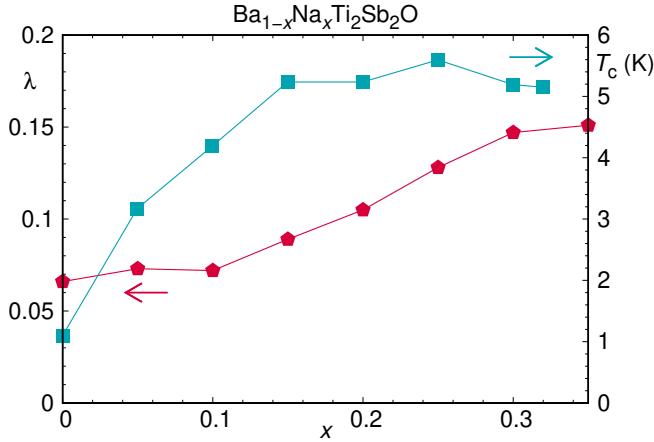


FIG. 6. (Color online) Leading eigenvalues  $\lambda$  of the gap equation as a function of doping level  $x$ .  $T_c$  data are from Ref. 9 and 20.

$\text{Ba}_{1-x}\text{Na}_x\text{Ti}_2\text{Sb}_2\text{O}$ . The eigenvalue  $\lambda$  increases as a function of alkali doping (Fig. 6), and follows the doping trend of the maxima in the susceptibility (Fig. 4(a)). Thus, the increase of  $T_c$  with alkali doping (Fig. 1) is clearly explained by the susceptibility trends rather than the density of states at the Fermi level. By performing the pairing calculations on 3D Fermi surfaces, we have verified that the sign-changing  $s$ -wave is indeed the dominating solution for all alkali doped materials  $\text{Ba}_{1-x}\text{A}_x\text{Ti}_2\text{Sb}_2\text{O}$  ( $\text{A}=\text{Na}, \text{K}, \text{Rb}$ ).

At low alkali doping levels we have found an order parameter, which contains nodes on the Fermi surface sheets around  $M$  and a relatively large gap on the central Fermi surface sheets around  $\Gamma$ . With increasing doping, the Fermi surface sheets around  $M$  become nodeless, but the reconstructed sheets around  $\Gamma$ , which are almost exclusively of  $\text{Sb } 5p$  character, are hardly gapped at all. Those strongly non-uniform order parameters need to

be taken into account when interpreting thermodynamic and other experiments trying to determine the symmetry of the superconducting state in titanium oxypnictides.

*Conclusions.*— We have investigated the electronic and superconducting properties of  $\text{Ba}_{1-x}\text{Na}_x\text{Ti}_2\text{Sb}_2\text{O}$  using density functional and spin fluctuation theory. We modeled the crystal structure evolution using an interpolation of experimental lattice parameters and a DFT predicted antimony position. The density of states at the Fermi level  $N(E_F)$  shows a trend which is in sharp contrast to the evolution of the superconducting  $T_c$ , indicating that transition temperatures may not be accounted for by an electron-phonon mechanism.

Although the band structure and density of states show that constituents of  $\text{Ba}_{1-x}\text{A}_x\text{Ti}_2\text{Sb}_2\text{O}$  ( $\text{A}=\text{Na}, \text{K}, \text{Rb}$ ) are strongly hybridized and many orbitals lie close to the Fermi level, we have found that the susceptibility is completely dominated by the  $\text{Ti } 3d_{xy}$  orbitals.

Proceeding on the assumption of a magnetic pairing mechanism, which has been suggested by an investigation into the nematicity of  $\text{BaTi}_2\text{Sb}_2\text{O}$  in Ref. 25, we find that we can satisfactorily explain the  $T_c$  trend with a spin fluctuation pairing mechanism. We find that a sign-changing  $s$ -wave order parameter with non-uniform gap size on the various Fermi surface sheets clearly dominates in  $\text{Ba}_{1-x}\text{Na}_x\text{Ti}_2\text{Sb}_2\text{O}$  at all doping levels. Explaining the nontrivial transition temperature trends of titanium based superconductors with isoelectronic doping and pressure are interesting future fields of study.

## ACKNOWLEDGMENTS

We acknowledge fruitful discussions with Yoshihiro Kubozono. Part of the computations were carried out at the Supercomputer Center at the Institute for Solid State Physics, the University of Tokyo. This work was supported by MEXT Leading Initiative for Excellent Young

- 
- [1] A. Adam and H.-U. Schuster, Darstellung und kristallstruktur der pnictidoxide  $\text{Na}_2\text{Ti}_2\text{As}_2\text{O}$  und  $\text{Na}_2\text{Ti}_2\text{Sb}_2\text{O}$ , *Z. Anorg. Allg. Chem.* **584**, 150 (1990).
- [2] E. Axtell, T. Ozawa, S. M. Kauzlarich, and R. R. Singh, Phase transition and spin-gap behavior in a layered tetragonal pnictide oxide, *J. Solid State Chem.* **134**, 423 (1997).
- [3] W. E. Pickett, Electronic instability in inverse- $\text{K}_2\text{NiF}_4$ -structure  $\text{Na}_2\text{Sb}_2\text{Ti}_2\text{O}$ , *Phys. Rev. B* **58**, 4335 (1998).
- [4] T. Yajima, K. Nakano, F. Takeiri, T. Ono, Y. Hosokoshi, Y. Matsushita, J. Hester, Y. Kobayashi, and H. Kageyama, Superconductivity in  $\text{BaTi}_2\text{Sb}_2\text{O}$  with a  $d^1$  square lattice, *J. Phys. Soc. Jpn.* **81**, 103706 (2012).
- [5] T. Yajima, K. Nakano, F. Takeiri, J. Hester, T. Yamamoto, Y. Kobayashi, N. Tsuji, J. Kim, A. Fujiwara, and H. Kageyama, Synthesis and physical properties of the new oxybismuthides  $\text{BaTi}_2\text{Bi}_2\text{O}$  and  $(\text{SrF})_2\text{Ti}_2\text{Bi}_2\text{O}$  with a  $d^1$  square net, *J. Phys. Soc. Jpn.* **82**, 013703 (2013).
- [6] T. Yajima, K. Nakano, F. Takeiri, Y. Nozaki, Y. Kobayashi, and H. Kageyama, Two superconducting phases in the isovalent solid solutions  $\text{BaTi}_2\text{Pn}_2\text{O}$  ( $\text{Pn} = \text{As, Sb, and Bi}$ ), *J. Phys. Soc. Jpn.* **82**, 033705 (2013).
- [7] H.-F. Zhai, W.-H. Jiao, Y.-L. Sun, J.-K. Bao, H. Jiang, X.-J. Yang, Z.-T. Tang, Q. Tao, X.-F. Xu, Y.-K. Li, C. Cao, J.-H. Dai, Z.-A. Xu, and G.-H. Cao, Superconductivity, charge- or spin-density wave, and metal-nonmetal transition in  $\text{BaTi}_2(\text{Sb}_{1-x}\text{Bi}_x)_2\text{O}$ , *Phys. Rev. B* **87**, 100502(R) (2013).
- [8] X. F. Wang, Y. J. Yan, J. J. Ying, Q. J. Li, M. Zhang, N. Xu, and X. H. Chen, Structure and physical properties for a new layered pnictide-oxide:  $\text{BaTi}_2\text{As}_2\text{O}$ , *J. Phys.: Condens. Matter* **22**, 075702 (2010).
- [9] P. Doan, M. Gooch, Z. Tang, B. Lorenz, A. Möller, J. Tapp, P. C. W. Chu, and A. M. Guloy,  $\text{Ba}_{1-x}\text{Na}_x\text{Ti}_2\text{Sb}_2\text{O}$  ( $0.0 \leq x \leq 0.33$ ): A layered titanium-based pnictide oxide superconductor, *J. Am. Chem. Soc.* **134**, 16520 (2012).
- [10] R. H. Liu, D. Tan, Y. A. Song, Q. J. Li, Y. J. Yan, J. J. Ying, Y. L. Xie, X. F. Wang, and X. H. Chen, Physical properties of the layered pnictide oxides  $\text{Na}_2\text{Ti}_2\text{P}_2\text{O}$  ( $\text{P}=\text{As, Sb}$ ), *Phys. Rev. B* **80**, 144516 (2009).
- [11] S. Kitagawa, K. Ishida, K. Nakano, T. Yajima, and H. Kageyama, *s*-wave superconductivity in superconducting  $\text{BaTi}_2\text{Sb}_2\text{O}$  revealed by  $^{121/123}\text{Sb}$ -NMR/nuclear quadrupole resonance measurements, *Phys. Rev. B* **87**, 060510(R) (2013).
- [12] F. von Rohr, A. Schilling, R. Nesper, C. Baines, and M. Bendele, Conventional superconductivity and charge-density-wave ordering in  $\text{Ba}_{1-x}\text{Na}_x\text{Ti}_2\text{Sb}_2\text{O}$ , *Phys. Rev. B* **88**, 140501(R) (2013).
- [13] Y. Nozaki, K. Nakano, T. Yajima, H. Kageyama, B. Frandsen, L. Liu, S. Cheung, T. Goko, Y. J. Uemura, T. S. J. Munsie, T. Medina, G. M. Luke, J. Munevar, D. Nishio-Hamane, and C. M. Brown, Muon spin relaxation and electron/neutron diffraction studies of  $\text{BaTi}_2(\text{As}_{1-x}\text{Sb}_x)_2\text{O}$ : Absence of static magnetism and superlattice reflections, *Phys. Rev. B* **88**, 214506 (2013).
- [14] U. Pachmayr and D. Johrendt, Superconductivity in  $\text{Ba}_{1-x}\text{K}_x\text{Ti}_2\text{Sb}_2\text{O}$  ( $0 \leq x \leq 1$ ) controlled by the layer charge, *Solid State Sci.* **28**, 31 (2014).
- [15] F. von Rohr, R. Nesper, and A. Schilling, Superconductivity in rubidium-substituted  $\text{Ba}_{1-x}\text{Rb}_x\text{Ti}_2\text{Sb}_2\text{O}$ , *Phys. Rev. B* **89**, 094505 (2014).
- [16] Y. Wang, X. Yang, T. Taguchi, H. Li, T. He, H. Goto, R. Eguchi, T. Miyazaki, Y.-F. Liao, H. Ishii, and Y. Kubozono, Preparation and characterization of superconducting  $\text{Ba}_{1-x}\text{Cs}_x\text{Ti}_2\text{Sb}_2\text{O}$ , and its pressure dependence of superconductivity, *Jpn. J. Appl. Phys.* **58**, 110603 (2019).
- [17] W. Ishii, T. Yajima, and Z. Hiroi, Electronic phase diagram of the titanium oxypnictide superconductor  $\text{BaTi}_2(\text{Sb}_{1-x}\text{Bi}_x)_2\text{O}$ , *J. Phys.: Conf. Ser.* **969**, 012052 (2018).
- [18] Y. Wang, H. Li, T. Taguchi, A. Suzuki, A. Miura, H. Goto, R. Eguchi, T. Miyazaki, Y.-F. Liao, H. Ishii, and Y. Kubozono, Superconducting behavior of  $\text{BaTi}_2\text{Bi}_2\text{O}$  and its pressure dependence, *Phys. Chem. Chem. Phys.* **22**, 23315 (2020).
- [19] B. Lorenz, A. M. Guloy, and P. C. W. Chu, Superconductivity in titanium-based pnictide oxide compounds, *Int. J. Mod. Phys. B* **28**, 1430011 (2014).
- [20] M. Gooch, P. Doan, Z. Tang, B. Lorenz, A. M. Guloy, and P. C. W. Chu, Weak coupling BCS-like superconductivity in the pnictide oxide  $\text{Ba}_{1-x}\text{Na}_x\text{Ti}_2\text{Sb}_2\text{O}$  ( $x = 0$  and  $0.15$ ), *Phys. Rev. B* **88**, 064510 (2013).
- [21] S. Kamusella, P. Doan, T. Goltz, H. Luetkens, R. Sarkar, A. Guloy, and H.-H. Klauss, CDW order and unconventional *s*-wave superconductivity in  $\text{Ba}_{1-x}\text{Na}_x\text{Ti}_2\text{Sb}_2\text{O}$ , *J. Phys.: Conf. Ser.* **551**, 012026 (2014).
- [22] S. Kitagawa, K. Ishida, W. Ishii, T. Yajima, and Z. Hiroi, Nematic transition and highly two-dimensional superconductivity in  $\text{BaTi}_2\text{Bi}_2\text{O}$  revealed by  $^{209}\text{Bi}$ -nuclear magnetic resonance/nuclear quadrupole resonance measurements, *Phys. Rev. B* **98**, 220507(R) (2018).
- [23] A. Subedi, Electron-phonon superconductivity and charge density wave instability in the layered titanium-based pnictide  $\text{BaTi}_2\text{Sb}_2\text{O}$ , *Phys. Rev. B* **87**, 054506 (2013).
- [24] D. J. Singh, Electronic structure, disconnected Fermi surfaces and antiferromagnetism in the layered pnictide superconductor  $\text{Na}_x\text{Ba}_{1-x}\text{Ti}_2\text{Sb}_2\text{O}$ , *New J. Phys.* **14**, 123003 (2012).
- [25] G. Zhang, J. K. Glasbrenner, R. Flint, I. I. Mazin, and R. M. Fernandes, Double-stage nematic bond ordering above double stripe magnetism: Application to  $\text{BaTi}_2\text{Sb}_2\text{O}$ , *Phys. Rev. B* **95**, 174402 (2017).
- [26] X.-L. Yu, D.-Y. Liu, Y.-M. Quan, T. Jia, H.-Q. Lin, and L.-J. Zou, A site-selective antiferromagnetic ground state in layered pnictide-oxide  $\text{BaTi}_2\text{As}_2\text{O}$ , *J. Appl. Phys.* **115**, 17A924 (2014).
- [27] H. Kim, J. H. Shim, K. Kim, and B. I. Min, Charge density waves and the Coulomb correlation effects in  $\text{Na}_2\text{Ti}_2\text{P}_2\text{O}$  ( $\text{P}=\text{Sb, As}$ ), *Phys. Rev. B* **96**, 155142 (2017).

- [28] G. Wang, H. Zhang, L. Zhang, and C. Liu, The electronic structure and magnetism of  $\text{BaTi}_2\text{Sb}_2\text{O}$ , *J. Appl. Phys.* **113**, 243904 (2013).
- [29] X.-W. Yan and Z.-Y. Lu, Layered pnictide-oxide  $\text{Na}_2\text{Ti}_2\text{Pn}_2\text{O}$  ( $\text{Pn}=\text{As}, \text{Sb}$ ): a candidate for spin density waves, *J. Phys.: Condens. Matter* **25**, 365501 (2013).
- [30] K. Koepernik and H. Eschrig, Full-potential nonorthogonal local-orbital minimum-basis band-structure scheme, *Phys. Rev. B* **59**, 1743 (1999).
- [31] J. P. Perdew, K. Burke, and M. Ernzerhof, Generalized gradient approximation made simple, *Phys. Rev. Lett.* **77**, 3865 (1996).
- [32] See Supplemental Material at <http://link.aps.org/supplemental/10.1103/PhysRevBXXX> for details on the crystal structure preparation, tight binding model and the electronic properties.
- [33] H. Eschrig and K. Koepernik, Tight-binding models for the iron-based superconductors, *Phys. Rev. B* **80**, 104503 (2009).
- [34] D. Guterding, H. O. Jeschke, P. J. Hirschfeld, and R. Valentí, Unified picture of the doping dependence of superconducting transition temperatures in alkali metal/ammonia intercalated FeSe, *Phys. Rev. B* **91**, 041112(R) (2015).
- [35] D. Guterding, *Microscopic modelling of organic and iron-based superconductors*, Ph.D. thesis, Goethe-Universität Frankfurt, Germany (2017).
- [36] M. Shimizu, N. Takemori, D. Guterding, and H. O. Jeschke, Two-dome superconductivity in FeS induced by a Lifshitz transition, *Phys. Rev. Lett.* **121**, 137001 (2018).
- [37] M. Shimizu, N. Takemori, D. Guterding, and H. O. Jeschke, Importance of the Fermi surface and magnetic interactions for the superconducting dome in electron-doped FeSe intercalates, *Phys. Rev. B* **101**, 180511(R) (2020).
- [38] H. Hosono, K. Tanabe, E. Takayama-Muromachi, H. Kageyama, S. Yamanaka, H. Kumakura, M. Nohara, H. Hiramatsu, and S. Fujitsu, Exploration of new superconductors and functional materials, and fabrication of superconducting tapes and wires of iron pnictides, *Sci. Technol. Adv. Mater.* **16**, 033503 (2015).
- [39] N. R. Davies, R. D. Johnson, A. J. Princep, L. A. Gannon, J.-Z. Ma, T. Qian, P. Richard, H. Li, M. Shi, H. Nowell, P. J. Baker, Y. G. Shi, H. Ding, J. Luo, Y. F. Guo, and A. T. Boothroyd, Coupled commensurate charge density wave and lattice distortion in  $\text{Na}_2\text{Ti}_2\text{Pn}_2\text{O}$  ( $\text{Pn}=\text{As}, \text{Sb}$ ) determined by x-ray diffraction and angle-resolved photoemission spectroscopy, *Phys. Rev. B* **94**, 104515 (2016).
- [40] Z. Huang, W. L. Liu, H. Y. Wang, Y. L. Su, Z. T. Liu, X. B. Shi, S. Y. Gao, Z. C. Jiang, Z. H. Liu, J. S. Liu, X. L. Lu, Y. C. Yang, J. X. Zhang, S. C. Huan, W. Xia, J. H. Wang, Y. S. Wu, X. Wang, N. Yu, Y. B. Huang, S. Qiao, J. Li, W. W. Zhao, Y. F. Guo, G. Li, and D. W. Shen, Dual topological superconducting states in the layered titanium-based oxypnictide superconductor  $\text{BaTi}_2\text{Sb}_2\text{O}$  (2020), arXiv:2009.06805.



# Theory for doping trends in titanium oxypnictide superconductors – Supplemental Material –

Han-Xiang Xu,<sup>1</sup> Daniel Guterding,<sup>2</sup> and Harald O. Jeschke<sup>1</sup>

<sup>1</sup>Research Institute for Interdisciplinary Science, Okayama University, Okayama 700-8530, Japan

<sup>2</sup>Fachbereich Mathematik, Naturwissenschaften und Datenverarbeitung,  
Technische Hochschule Mittelhessen, Wilhelm-Leuschner-Straße 13, 61169 Friedberg, Germany

(Dated: August 24, 2021)

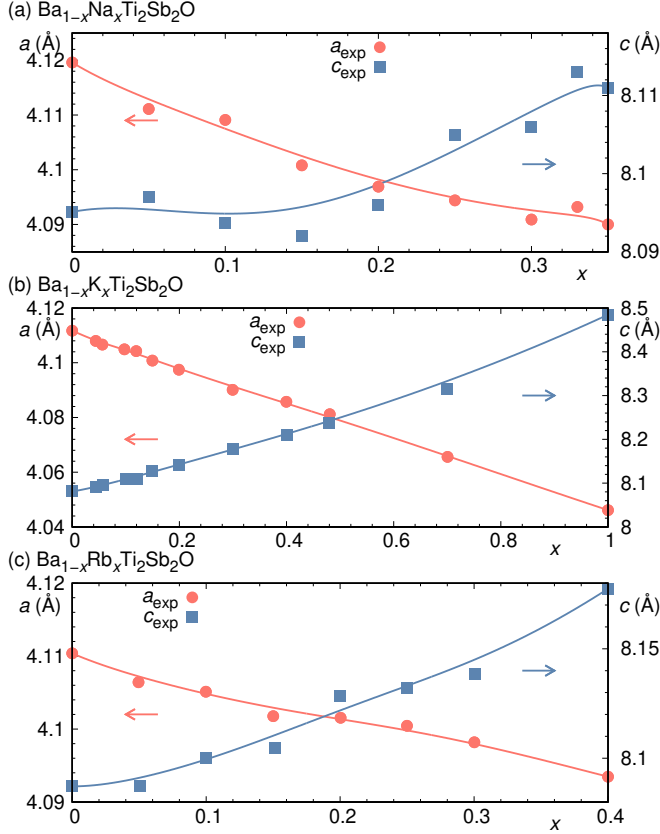


FIG. S1. Interpolation of experimental lattice constants.

## I. CRYSTAL STRUCTURES

We use experimental lattice parameters for  $\text{Ba}_{1-x}\text{Na}_x\text{Ti}_2\text{Sb}_2\text{O}$  from Ref. 1, for  $\text{Ba}_{1-x}\text{K}_x\text{Ti}_2\text{Sb}_2\text{O}$  from Ref. 2 and for  $\text{Ba}_{1-x}\text{Rb}_x\text{Ti}_2\text{Sb}_2\text{O}$  from Ref. 3. They are shown as symbols in Fig. S1. We smoothly interpolate the lattice parameters in order to sample the doped crystal structures at regular intervals. The antimony positions are the only free positions in the  $P4/mmm$  crystal structures, and we obtain them by relaxation using FPLO basis [4] and GGA exchange correlation functional. We model the alkali doping  $x$  by using the virtual crystal approximation for Ba, using a nuclear charge between  $Z = 55$  and  $56$ .

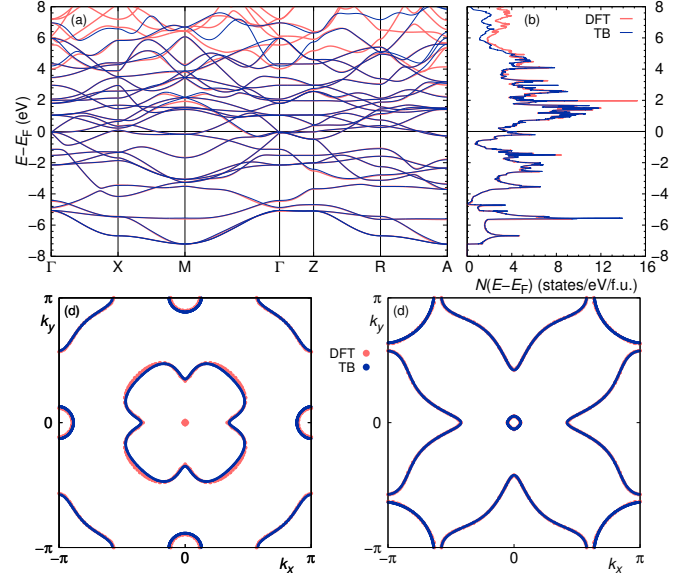


FIG. S2. Comparison between density functional theory and tight binding model for  $\text{BaTi}_2\text{Sb}_2\text{O}$ . (a) Band structure, (b) density of states, (c) Fermi surface at  $k_z = 0$  and (d) Fermi surface at  $k_z = \pi$ . The agreement is excellent.

## II. TIGHT BINDING MODEL

We use projective Wannier functions within FPLO [5] to construct faithful tight binding models of  $\text{BaTi}_2\text{Sb}_2\text{O}$  and the alkali doping series. Fig. S2 shows the quality of fit for band structure, density of states and Fermi surface of  $\text{BaTi}_2\text{Sb}_2\text{O}$ ; the agreement is nearly perfect. To achieve this, we need to include 26 orbitals: Ten Ti  $3d$  orbitals, two Ti  $4s$  orbitals, six Sb  $5p$  orbitals, five Ba  $5d$  orbitals and three O  $2p$  orbitals.

## III. ELECTRONIC STRUCTURE

Figure S3 shows the weight of all  $3d$  orbitals of Ti1 for  $\text{BaTi}_2\text{Sb}_2\text{O}$ . The Ti2  $3d$  orbitals have weights which are 90 degree rotated with respect to Ti1 (not shown). The dominating orbital is Ti  $3d_{xy}$ , and  $3d_{xz}$ ,  $3d_{yz}$  orbitals have some weight at the Fermi level as well.  $3d_{z^2}$  and  $3d_{x^2-y^2}$  orbitals contributions are negligibly small.

Figure S4 shows the Fermi surface of  $\text{Ba}_{1-x}\text{Na}_x\text{Ti}_2\text{Sb}_2\text{O}$  at  $x = 0.05$  and compares fa-

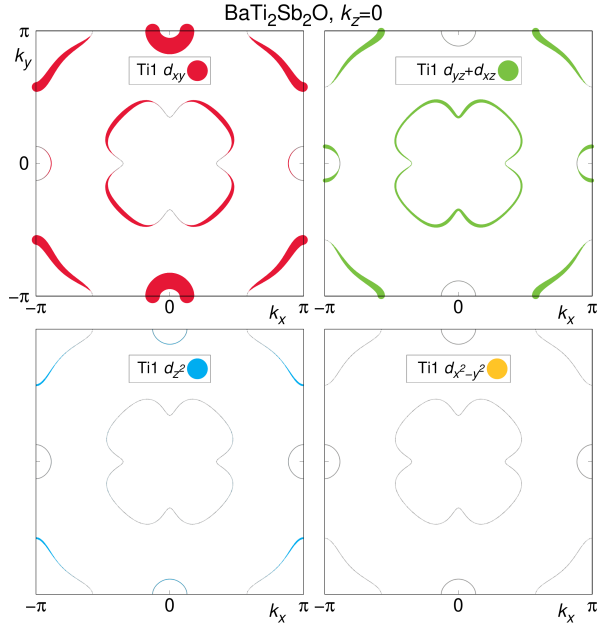


FIG. S3. 2D Fermi surface of  $\text{BaTi}_2\text{Sb}_2\text{O}$  with Ti 3d orbital character. All weights are shown with the same scale.  $3d_{xy}$  clearly dominates, followed in importance by  $3d_{yz}/3d_{xz}$ .  $3d_{z^2}$  is very faint, and  $3d_{x^2-y^2}$  character is negligible. Weights of the second Ti site are 90 degree rotated with respect to the first so that the sum has the  $C_4$  symmetry of the space group.

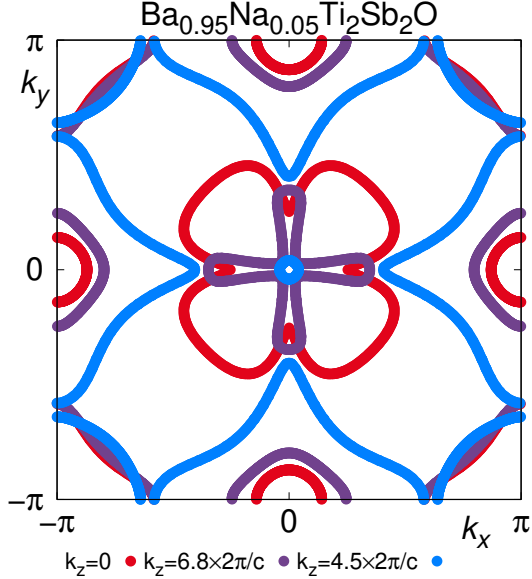


FIG. S4. Fermi surface of  $\text{Ba}_{0.95}\text{Na}_{0.05}\text{Ti}_2\text{Sb}_2\text{O}$  at  $k_z = 0$ ,  $k_z = 0.5\pi$  and  $k_z = \pi$ , calculated within GGA.

vorably with the angle resolved photoemission (ARPES) experiment of Ref. [6].

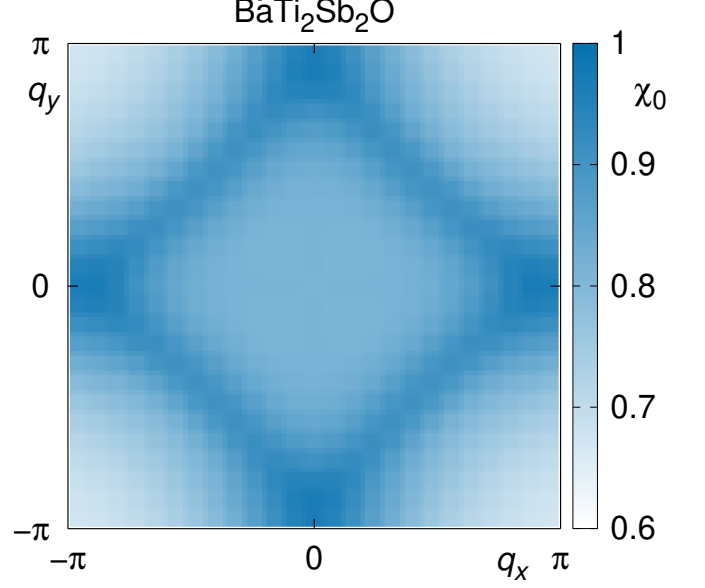


FIG. S5. Non-interacting susceptibility  $\chi_0$  for  $\text{BaTi}_2\text{Sb}_2\text{O}$ .

#### IV. NON-INTERACTING SUSCEPTIBILITY

The non-interacting susceptibility  $\chi_0$  is shown in Fig. S5. This is based on a 3D calculation of  $\chi_0$  on a  $25 \times 25 \times 9$  grid using a  $25 \times 25 \times 9$  integration grid. The  $q_z = 0$  cut shown in Fig. S5 is extracted using a  $100 \times 100$  interpolation grid. The same interpolation grid was used for the interacting susceptibility  $\chi_s$  shown in the main text, Fig. 5 (a).

[1] P. Doan, M. Gooch, Z. Tang, B. Lorenz, A. Möller, J. Tapp, P. C. W. Chu, and A. M. Guloy,  $\text{Ba}_{1-x}\text{Na}_x\text{Ti}_2\text{Sb}_2\text{O}$  ( $0.0 \leq x \leq 0.33$ ): A layered titanium-based pnictide oxide superconductor, J. Am. Chem. Soc. **134**, 16520 (2012).

[2] U. Pachmayr and D. Johrendt, Superconductivity in  $\text{Ba}_{1-x}\text{K}_x\text{Ti}_2\text{Sb}_2\text{O}$  ( $0 \leq x \leq 1$ ) controlled by the layer charge, Solid State Sci. **28**, 31 (2014).  
[3] F. von Rohr, R. Nesper, and A. Schilling, Superconductivity in rubidium-substituted  $\text{Ba}_{1-x}\text{Rb}_x\text{Ti}_2\text{Sb}_2\text{O}$ , Phys.



- Rev. B **89**, 094505 (2014).
- [4] K. Koepernik and H. Eschrig, Full-potential nonorthogonal local-orbital minimum-basis band-structure scheme, Phys. Rev. B **59**, 1743 (1999).
- [5] H. Eschrig and K. Koepernik, Tight-binding models for the iron-based superconductors, Phys. Rev. B **80**, 104503 (2009).
- [6] N. R. Davies, R. D. Johnson, A. J. Princep, L. A. Gannon, J.-Z. Ma, T. Qian, P. Richard, H. Li, M. Shi, H. Nowell, P. J. Baker, Y. G. Shi, H. Ding, J. Luo, Y. F. Guo, and A. T. Boothroyd, Coupled commensurate charge density wave and lattice distortion in  $\text{Na}_2\text{Ti}_2\text{Pn}_2\text{O}$  ( $\text{Pn}=\text{As}, \text{Sb}$ ) determined by x-ray diffraction and angle-resolved photoemission spectroscopy, Phys. Rev. B **94**, 104515 (2016).